

Energy & Environmental Science

Accepted Manuscript



This is an *Accepted Manuscript*, which has been through the Royal Society of Chemistry peer review process and has been accepted for publication.

Accepted Manuscripts are published online shortly after acceptance, before technical editing, formatting and proof reading. Using this free service, authors can make their results available to the community, in citable form, before we publish the edited article. We will replace this *Accepted Manuscript* with the edited and formatted *Advance Article* as soon as it is available.

You can find more information about *Accepted Manuscripts* in the [Information for Authors](#).

Please note that technical editing may introduce minor changes to the text and/or graphics, which may alter content. The journal's standard [Terms & Conditions](#) and the [Ethical guidelines](#) still apply. In no event shall the Royal Society of Chemistry be held responsible for any errors or omissions in this *Accepted Manuscript* or any consequences arising from the use of any information it contains.

Cite this: DOI: 10.1039/c0xx00000x

www.rsc.org/xxxxxx

ARTICLE TYPE

An Organic Ionic Plastic Crystal Electrolyte for Rate Capability and Stability of Ambient Temperature Lithium Batteries[†]

Liyu Jin,^{ab} Patrick C. Howlett,^{*bc} Jennifer M. Pringle,^{bc} Judith Janikowski,^{ab} Michel Armand,^e Douglas R. MacFarlane^{bd} and Maria Forsyth^{bc}

Received (in XXX, XXX) Xth XXXXXXXXXX 20XX, Accepted Xth XXXXXXXXXX 20XX

DOI: 10.1039/b000000x

^a Department of Materials Engineering, Monash University, Clayton, Victoria 3800, Australia^b ARC Centre of Excellence for Electromaterials Science^c Institute for Frontier Materials, Deakin University, Burwood Campus, Burwood, Victoria 3125, Australia.

E-mail: patrick.howlett@deakin.edu.au

^d School of Chemistry, Monash University, Clayton, Victoria 3800, Australia^e CIC Energigune Energy Cooperative Research Centre, C/Albert Einstein 48 CP 01510 Minano, Spain[†] Electronic Supporting Information available: the enlarged synchrotron powder x-ray diffraction pattern plots, additional CV analysis and example Nyquist Plots used to determine conductivity.

Abstract

Reliable, safe and high performance solid electrolytes are a critical step in the advancement of high energy density secondary batteries. In the present work we demonstrate a novel solid electrolyte based on the organic ionic plastic crystal (OIPC) triisobutyl(methyl)phosphonium bis(fluorosulfonyl)imide (P₁₄₄₄FSI). With the addition of 4 mol% LiFSI, the OIPC shows a high conductivity of 0.26 mS cm⁻¹ at 22 °C. The ion transport mechanisms have been rationalized by compiling thermal phase behaviour and crystal structure information obtained by variable temperature synchrotron X-ray diffraction. With a large electrochemical window (*ca.* 6 V) and importantly, the formation of a stable and highly conductive solid electrolyte interphase (SEI), we were able to cycle lithium cells (Li | LiFePO₄) at 30 °C and 20 °C at rates of up to 1 C with good capacity retention. At the 0.1 C rate, about 160 mAh g⁻¹ discharge capacity was achieved at 20 °C, which is the highest for OIPC based cells to date. It is anticipated that these small phosphonium cation and [FSI] anion based OIPCs will show increasing significance in the field of solid electrolytes.

Introduction

In the development of safer electrolytes for lithium ion/metal batteries,²⁻⁸ Organic Ionic Plastic Crystals (OIPCs) are particularly appealing. With relative strong ionic bonding between charged species, they are commonly non-flammable and non-volatile. Furthermore, as solid and plastic materials they can relieve leakage concerns, allow a variety of cell shapes, simplify material handling and potentially be integrated into 3D printing technologies. Plastic crystals are often also referred to as rotational crystalline phases⁹⁻¹¹ due to the fact that, within long-range ordered crystalline structures, they embody orientational and/or rotational short-range molecular motions. These motions confer solid electrolyte materials with the highly desired combination of mechanical flexibility^{12,13} and rapid ion transport. This set of desired properties cannot be easily achieved in common solid electrolytes based on either ceramic, glass or polymer electrolytes. Conse-

quently, OIPCs have been increasingly recognized as potential solid ion conductors for electrochemical devices such as batteries,^{2-8,12,14-24} supercapacitors,^{9-11,25} fuel cells,^{12,13,26-31} and dye sensitized solar cells.^{24,32-37}

Another advantage of OIPCs is that like ionic liquids (ILs), the physical and chemical properties can be tailored by selectively combining cations and anions. Since the pioneering research into OIPCs as solid electrolytes in 1986,³⁸ researchers have been seeking, modifying and developing cations^{11,12,16,39,40}, anions^{12,41-43} and their combinations to pursue competitive cell performance. This requires electrolytes with a suitable plastic phase range, wide electrochemical window and high ionic conductivity. Nevertheless, very few combinations have thus far been found to give practical cell performance, particularly at ambient temperature.

At ambient temperature, one of the limiting factors is the low ionic conductivity of OIPCs even with the addition of lithium salt, because Phase I generally occurs at higher temperatures. It is

common for OIPCs to have several phases, and by convention, the phase just below the melting point is denoted as Phase I. This is the most “plastic” and conductive phase (with one known exception⁴⁴). Moreover, with certain lithium salt additions, it is usually Phase I that exhibits sufficient conductivity for practical applications (*i.e.* $>10^{-4}$ S cm⁻¹). Unfortunately, popular pyrrolidinium¹¹, imidazolium⁴⁵ and ammonium^{46,47} based cations with short alkyl chains (up to two carbons) commonly form OIPCs with a higher-than-ambient Phase I (and with long alkyl chains they usually form room temperature ionic liquids⁴⁸). This is particularly the case when the anions are structurally simple, such as [PF₆], [BF₄], or [N(CN)₂]. Some of these OIPCs have Phase I onset temperatures above 150 °C⁴⁶ and therefore it is the less plastic or even rigid phases (*i.e.* normal insulating crystal phases) that occur at ambient temperature. Consequently, the lack of short-range disorder undermines both the mechanical flexibility and ionic conductivity.

Therefore, over the last decade, a major search for alternative cations or anions has been undertaken to realize functional lithium cells using OIPCs at ambient temperature. Alarco *et al.* reported a series of new OIPCs based on pyrazolium imide cations and the bis(trifluoromethanesulfonyl)imide ([NTf₂]) anion.²¹ Some of these new OIPCs show Phase I at room temperature and are highly conductive. By adding LiNTf₂ into one of OIPCs (*N,N'*-diethyl-3-methylpyrazolium NTf₂), they were able to cycle cells with LiFePO₄ | Li₄Ti₅O₁₂ electrodes at ambient and even lower-than-ambient temperatures. However, the cell capacities, especially at higher currents, were relatively low, and it appears that this pyrazolium based cation suffers from low cathodic stability.¹⁶ Recently, two novel OIPCs were found to have conductive phases at ambient-temperature. One is from the series based on the fluorohydrogenate ([F(H)F]) anion⁴³ (with *N,N*-dimethyl pyrrolidinium as the cation); the other is from the series based on the cyanate ([OCN⁻]) anion (with *N*-ethyl-*N*-methyl pyrrolidinium as the cation).⁴⁹ Unfortunately, both of these OIPCs have narrow electrochemical windows (electrochemical windows of some cyanate based OIPCs were recently tested but not published). In 2007, Zhou *et al.* found that Li[CF₃BF₃] doped *N,N*-diethyl-*N*-methyl-*N*-(*n*-propyl)ammonium trifluoromethyltrifluoroborate ([N₁₂₂₃][CF₃BF₃]) had high conductivity at room temperature as well as sufficiently wide electrochemical window.¹² Thus, this material could also be useful for lithium battery development.

Triisobutylmethylphosphonium bis(fluorosulfonyl)imide (P₁₄₄₄FSI), which has a suitable plastic phase range (10 – 37 °C), was discovered in our recent work developing a series of novel OIPCs using small phosphonium cations.⁴⁰ In general, compared to their quaternary ammonium analogues (*e.g.* imidazolium, tetraalkylammonium and pyrrolidinium), phosphonium based OIPCs have been much less studied. Nevertheless, phosphonium based ILs can have higher thermal and electrochemical stability than their ammonium analogues,⁵⁰ and some phosphonium ILs are already being synthesized on an industrial scale.^{51,52} The [FSI] anion has been patented for commercial use in the form of ionic liquid electrolytes.^{53,54} As a result of delocalization of the negative charge on this anion,⁵⁵ the weak ionic interactions in the ILs decreases the viscosity and increases the conductivity, which is particularly favourable for battery electrolyte development when high rate performance is pursued. Furthermore, the [FSI] anion

seems to support long-term cycling of the deposition/stripping process on lithium metal very well;^{56,57} this is closely related to the formation of a stable and conductive solid electrolyte interphase (SEI).⁵⁸ Good capacity retention of several cathode materials (*e.g.* LiCoO₂⁵⁹, LiFePO₄⁶⁰⁻⁶²) has also been seen in some [FSI] based ionic liquid electrolytes.

In this work, we present lithium (Li | LiFePO₄) cells using a solid electrolyte consisting of 4 mol% LiFSI in P₁₄₄₄FSI; the cells realize high capacity retention and rate capability cycling at ambient temperature. We ascribe this outstanding performance to the doped OIPC, which has a large electrochemical window, high ionic conductivity and the ability to form a stable and conductive SEI on the lithium metal surface. Analysis of the thermal and structural characteristics of the pure and doped OIPCs also provides insights into the origins of this superior electrolyte performance.

Experimental

Materials synthesis and melt doping

Triisobutylmethylphosphonium bis(fluorosulfonyl)imide (P₁₄₄₄FSI) was synthesized from triisobutylmethylphosphonium tosylate purchased from CYTEC[®] and potassium bis(fluorosulfonyl)imide purchased from Fluolyte (Suzhou Fluolyte Co., Ltd.) following a previously published route⁴⁰. Lithium bis(fluorosulfonyl)imide (LiFSI) salt was purchased from Solvionic[®], France (purity > 99%) and used as received. Addition of LiFSI to P₁₄₄₄FSI was performed in an argon filled glove box. LiFSI powder was added to liquid P₁₄₄₄FSI (m.p. 37 °C) at 60 °C and the mixture was stirred for 20 min to obtain a clear solution, before being allowed to solidify at room temperature.

Differential scanning calorimetry (DSC)

DSC was performed on a TA-Q100 instrument. All samples were weighed and sealed in aluminium pans under N₂ atmosphere. The samples were first cooled from room temperature to –20 °C, and subsequently heated to 60 °C at a rate of 2 °C/min. The first run was performed to minimize effects of different thermal histories of the samples on the DSC traces. The DSC results presented in this paper were collected from the second cooling and heating cycle.

Synchrotron X-ray powder diffraction

Samples were loaded into 0.5 mm Boron-Rich glass capillaries (Charles Supper Company Inc., Natick, MA) within an argon-filled glove box and an airtight seal was formed by melting the open end of each capillary. Variable temperature measurements were conducted isothermally (2 °C/min ramping and 5min isothermal time at each target temperature) using the Australian Synchrotron, Powder Diffraction Beamline in transmittance mode, at a wavelength of 1.2381 Å. The standard NIST LaB₆ (*a* = 4.15689 Å, Pm3m), *ca.* 2 to 40 μm size, was used for calibration.

Electrochemical impedance spectroscopy (EIS)

Ionic conductivity was measured by ac impedance spectroscopy on a Solartron[®] SI1260 impedance/gain phase analyser, which was connected to a Solartron[®] 1296 dielectric interface. A platinum-wire cell (two electrodes) was used for EIS measurements,

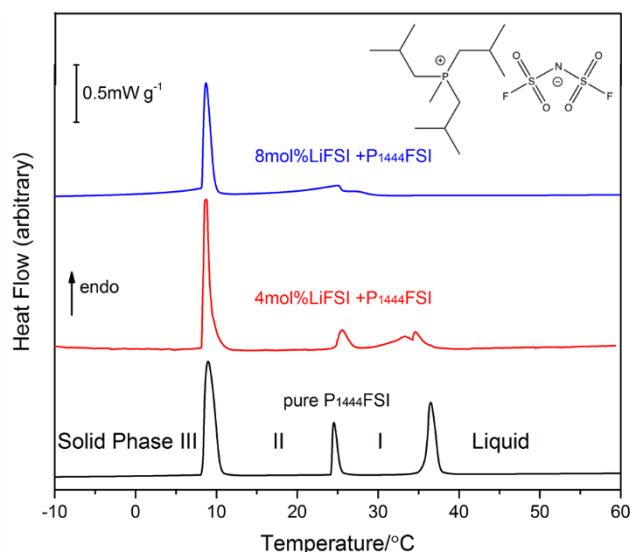


Fig 1. The DSC traces (second heating cycle) of pure P₁₄₄₄FSI, 4 and 8 mol% LiFSI doped P₁₄₄₄FSI. The insert image shows the chemical structure of P₁₄₄₄FSI.

with the cell constants calibrated with 0.01 M KCl solution. All samples were packed and sealed in a nitrogen atmosphere. Data was collected over a frequency range from 10 MHz to 1 Hz using a signal amplitude of 0.1 V at temperatures ranging from -20 to 60 °C at 5 °C intervals. The cell temperature was controlled by a Eurotherm[®] 2204, within 0.1 °C tolerance. The ramp rate was about 0.33 °C/min, and the samples were held at each temperature for 5 min to equilibrate prior to measurement.

Cyclic voltammetry

Cyclic voltammetry was performed using a Bio-Logic[®] SP-200 potentiostat in an argon-filled glove box. The cyclic voltammograms were acquired using a two-electrode cell setup, which is effective for solid or highly viscous samples and requires minimal amount of sample. The electrochemical window of the pure liquid P₁₄₄₄FSI was measured by soaking a piece of polyethylene separator (MTI[®] battery grade, 18 mm in diameter) in melted OIPC. The composite was sandwiched between a platinum working electrode with active surface area of 0.0078 cm² (1 mm in diameter) and a platinum counter/reference disk electrode with active surface area of 2.54 cm² (18 mm in diameter). In this configuration, the counter disk electrode also effectively acts as a quasi-reference electrode. The oxidation and reduction reactions were carried out in separate runs with fresh samples at 60 °C (on a hot-plate inside the glove box) with freshly prepared working and counter/reference electrodes (polished with 0.05 μm alumina powder and rinsed in distilled water). The platinum quasi reference potential was further calibrated using the ferrocene (Fc)/ferricinium (Fc⁺) redox couple dissolved in the OIPC ($E_{\text{Fc}^+/\text{Fc}} = 0.2 \text{ V vs. } E_{\text{P}})$. The same electrode configuration but using copper as the working and lithium metal as the counter/quasi reference electrode was used to study the Li⁺/Li redox behaviour after the addition of 4 mol% LiFSI to the OIPC, measured at 20 °C, *i.e.*, when the doped OIPC was solid. The conversion factor between $E_{\text{Li}^+/\text{Li}}$ and $E_{\text{Fc}^+/\text{Fc}}$ is -3.6 V *i.e.* $E_{\text{Li}^+/\text{Li}} = -3.6 \text{ V vs. } E_{\text{Fc}^+/\text{Fc}}$, used for the discussion, is an estimation based on the literature^{63,64}.

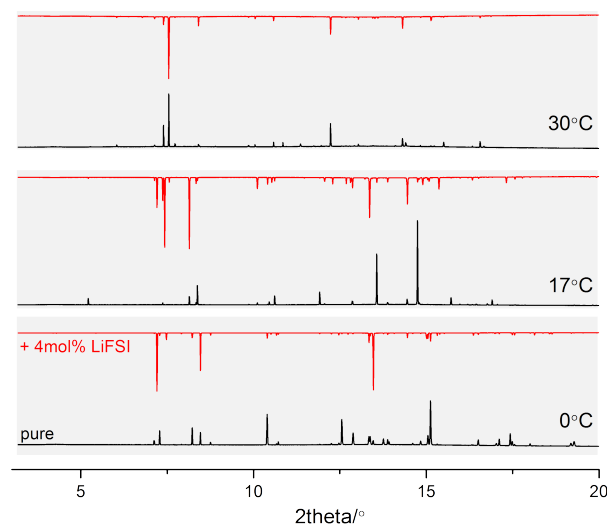


Fig 2. Variable temperature synchrotron X-ray diffraction patterns obtained for pure P₁₄₄₄FSI (black) and 4 mol% LiFSI doped P₁₄₄₄FSI (red and upside-down) at 0, 17 and 30 °C.

Li|LiFePO₄ coin cell cycling

Before assembly, lithium metal discs (10 mm in diameter) were punched from a 0.3 mm lithium strip (Sigma Aldrich[®]) and used as received. The LiFePO₄ cathode (10 mm in diameter) was dried under vacuum at 55 °C overnight. The LiFePO₄ loading was 1.5-2 mg cm⁻² (75% active material, 15% acetylene black and 10% polyvinylidene fluoride). To prepare the composite electrolyte, a polyethylene separator (MTI[®]) was soaked in the melted OIPC at 60 °C. After the separator was fully wetted, the temperature was reduced to 19 ± 1 °C and the composite solidified. Coin cells (2016, MTI[®]) were assembled inside an argon-filled glove box. Cell cycling tests were performed using a Biologic[®] VMP3/Z potentiostat controlled by EC-lab[®] (V.10.12) software inside a Heraeus 6000 series oven controlled to ±0.5 °C. The voltage cut-offs were set to 3.8 V for charging and 2.8 V for discharging. The impedance measurements for pristine cells were conducted at open circuit before charging for the first time and the cell voltages were about 3 V. The *in situ* impedance measurements were conducted after the cells were fully discharged and the voltage had recovered to about 3.1 V after resting at open circuit for 3 minutes.

Results and discussion

Thermal phase behaviour

Table 1. The thermal phase behaviour of pure and doped P₁₄₄₄FSI, as determined by DSC (Temperatures at the maximum of the peaks are reported).

Samples	Phase III – II		II – I		I – melt	
	Temperature/°C Entropy/J mol ⁻¹ K ⁻¹					
Pure P ₁₄₄₄ FSI	8.3	52	24.2	11	37.1	24
+4 mol%	8.2	40	24.8	5	34.6	-*
+8 mol%	8.1	25	25.0	-*	27.4	-*

* Entropy is not included due to poorly defined peak.

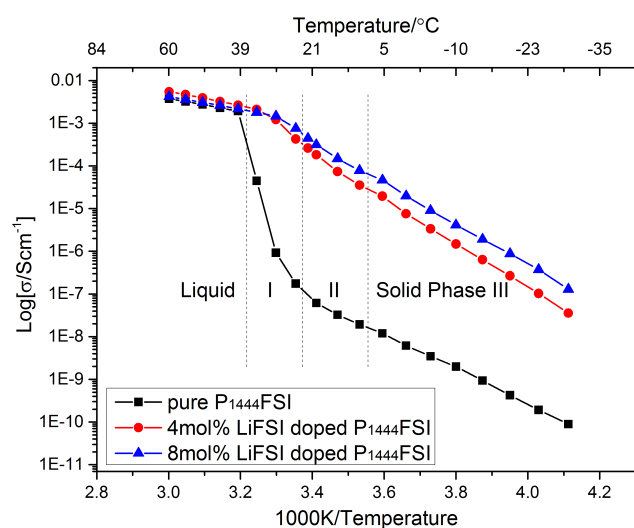


Fig 3. Temperature dependent conductivity data acquired for pure, 4 and 8mol% LiFSI doped P_{1444} FSI. Each phase is labelled and the transition temperatures of pure P_{1444} FSI are marked by dashed lines. Example Nyquist plots are shown in the ESI Fig S5-S12.

The thermal behaviour, evaluated by DSC, of the pure P_{1444} FSI sample together with the 4 and 8 mol% LiFSI doped samples is shown in Figure 1, and the transition temperatures and entropy data are summarized in Table 1. The phase behaviour of the pure sample has been previously published by our group,⁴⁰ and was reproduced here with the new batch of material. The pure material undergoes two sharp solid-solid phase transitions before the well-defined melting point of 37.1 °C, where it releases only 24 J mol⁻¹ K⁻¹ melting entropy. Based on its waxy nature and Timmermans' criterion for molecular plastic crystals¹⁰ and later observations^{6,11} for ionic plastic crystals, we consider this material to be a typical plastic crystal exhibiting two plastic crystal phases after a major transition at 8°C: Phase II (from 8 to 24 °C) and Phase I (from 24 to 36 °C).

The thermal phase behaviour is changed significantly in the 4 mol% LiFSI doped system. There is a new and broad peak emerging just before the final melting of the material at 34.6 °C. This new peak could be associated with the melting of a lithium-enriched phase created by the addition of lithium salt; this formation of a new compound when an alkali metal salt is mixed with an OIPC has previously been discussed.^{65,66} Meanwhile, the entropy of the transition from Phase III to II decreases by 23 % compared with that of the pure sample. This suggests that the lithium-enriched phase may not participate in this transition and that some amorphous phase may also be present. As the LiFSI salt content in the system was increased (to 8 mol%), the melting point decreased to below 30 °C so much so that it is likely that the observed broad peak also incorporates the melting of lithium-

enriched phase. Therefore, further investigations were focused on the pure and the 4 mol% LiFSI doped plastic crystals for both fundamental studies and application development.

To obtain greater insight into the temperature dependent phase behaviour, we also measured the variable temperature synchrotron X-ray diffraction patterns of both pure and 4 mol% LiFSI doped samples, as shown in Figure 2. The diffraction patterns in Phase III (0 °C) and Phase II (17 °C) exhibit large differences between the pure and doped samples and from the enlarged versions of Fig 2 (Fig S1, S2, S3 included in ESI), some additional new peaks clearly appeared in the 4 mol% LiFSI doped sample at both 0 °C and 17 °C. However, the highest temperature diffraction patterns (in Phase I at 30 °C) are very similar. The different diffraction intensities at some 2theta positions may be a result of orientational variability of the crystals in the capillaries.

The DSC analysis and X-ray diffraction patterns suggest that the addition of just 4 mol% Li salt to the OIPC results in the presence of at least two phases (compositional phases, not to be confused with plastic crystal phases) in the Phase III and II temperature regions: the pure OIPC (or possibly an OIPC-rich solid solution with some Li dissolved in the matrix) and a lithium-enriched phase. The additional peaks in the XRD pattern suggest that a second phase, most likely the lithium-enriched phase, has a quite different crystal structure from that of the pure OIPC. Thus, we probably observed mixed reflection peaks from both compositional phases in the 0 °C and 17 °C (Phase III and Phase II) diffraction patterns. However, at 30 °C (in Phase I for the OIPC) both XRD patterns only reflect the pure OIPC phase, suggesting that the lithium rich phase has melted, which is consistent with the DSC analysis. This melting behaviour could be a result of a eutectic reaction, as observed in some other OIPC systems,^{18,26,66,67} however, additional thermal analysis at multiple Li salt compositions would be needed to confidently describe the phase behaviour of this OIPC-Li system.

Conduction mechanisms

The ionic conductivity of the pure and LiFSI (4 and 8 mol%) containing plastic crystals was measured over a temperature range of -30 to 60 °C (Figure 3). The increase in conductivity moving from the pure to mixed systems is greater than that between the two lithium-salt containing ones, which display relatively similar values. Here, we discuss the conduction mechanisms for the different phases.

- 1) Rigid conventional crystal phase (-30 – 5 °C): the pure material has low conductivity in this phase. However, after the addition of 4 or 8 mol% LiFSI, the conductivity increases remarkably, by more than 3 orders of magnitude. This jump in the conductivity suggests that the lithium-enriched phase discussed above is highly conductive. However the presence of an amorphous phase may also contribute to this high conductivity.

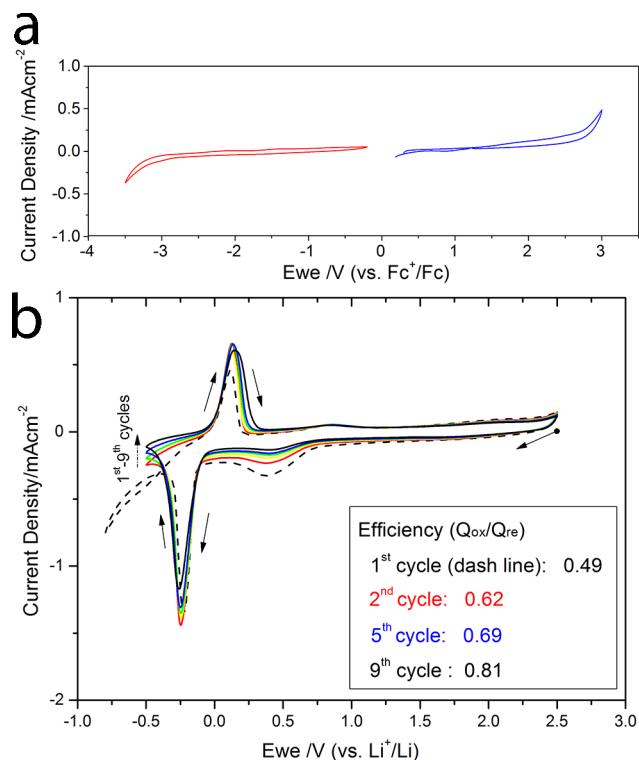


Fig 4. (a) Cyclic voltammogram of pure $P_{1444}FSI$ at $50\text{ }^{\circ}C$ with a scan rate of 100 mVs^{-1} . Working and reference/counter electrode were both Pt, which was calibrated by internal Fc^{+}/Fc reference (The conversion factor: $E_{Fc^{+}/Fc} = 0.2\text{ V vs. }E_{Pt}$). **(b)** Cyclic voltammograms of $4\text{ mol}\%$ LiFSI doped $P_{1444}FSI$ at $20\text{ }^{\circ}C$ with a scan rate of 50 mVs^{-1} . Only 1^{st} - 5^{th} cycles and 9^{th} cycle (dashed line) are shown. The lithium plating and stripping efficiency of each cycle was calculated from integration of reduction (Q_{red}) and oxidation (Q_{ox}) peaks. Working electrode was copper and reference/counter electrode was lithium.

- 2) Plastic crystal phases ($10 - 35\text{ }^{\circ}C$): the $4\text{ mol}\%$ LiFSI doped OIPC with the presence of a lithium-enriched phase and an increasingly conductive OIPC phase, has up to 3.5 orders of magnitude increase in conductivity in Phase II compared to the pure material, reaching 0.26 mS cm^{-1} at $22\text{ }^{\circ}C$. In Phase I, because of the melting and possible percolation along

grain boundaries of the lithium-enriched phase, there is rather low activation energy for ion transport compared to that of the pure sample. Despite the likely existence of a liquid component, the doped OIPCs as a whole have a soft but still solid-like nature at this temperature. This significant increase in conductivity by percolated liquid domains has also been recently discussed by Henderson *et al.*¹⁸

- 3) In the ionic liquid phase (above $40\text{ }^{\circ}C$ for the pure sample and $35\text{ }^{\circ}C$ after lithium addition): both the mixed and pure systems have similar conductivities, around 2.0 mS cm^{-1} at $40\text{ }^{\circ}C$, which is comparable to that of *N*-propyl-*N*-methylpyrrolidinium FSI ionic liquid.⁵⁶

Electrochemical behaviour

- As key properties for lithium battery electrolytes, the electrochemical stability and Li^0/Li^+ redox behaviour were investigated by cyclic voltammetry in pure $P_{1444}FSI$ and with $4\text{ mol}\%$ LiFSI added. Figure 4.a shows the voltammograms of the pure $P_{1444}FSI$, consisting of separate reduction and oxidation scans. The cathodic limit is *ca.* $-3.2\text{ V vs. ferrocene/ferrocenium } (Fc/Fc^+)$, which is in a good agreement with that of other quaternary phosphonium ILs^{40,50,68}. For most ILs with electrochemically stable anions such as $[PF_6]$, $[BF_4]$, $[NTf_2]$, $[FSI]$, it is generally believed that the reduction potentials of the cationic species determine the cathodic limit of the IL. In this case, in addition to literature data,^{40,50,69} our present observation confirms that the phosphonium cation with small alkyl chains has a high cathodic limit, superior to that of imidazolium^{70,71} and quaternary ammonium^{72,68} cation based ILs, and approaching those of pyrrolidinium¹¹ or piperidinium⁷¹ cation based ILs.

The pure plastic crystal has anodic limit above *ca.* $6\text{ V vs. }Li^+/Li$ ($2.4\text{ V vs. }Fc^+/Fc$), which makes it an interesting candidate for further development with high voltage cathodes.^{73,74} Nevertheless, it worth noting that compared with similar small phosphonium ILs with the NTf_2 anion,^{40,50} the FSI anion is usually oxidized at a slightly lower potential, which is consistent with the lower thermal stabilities of these ILs compared to those containing the NTf_2 anion.^{40,72}

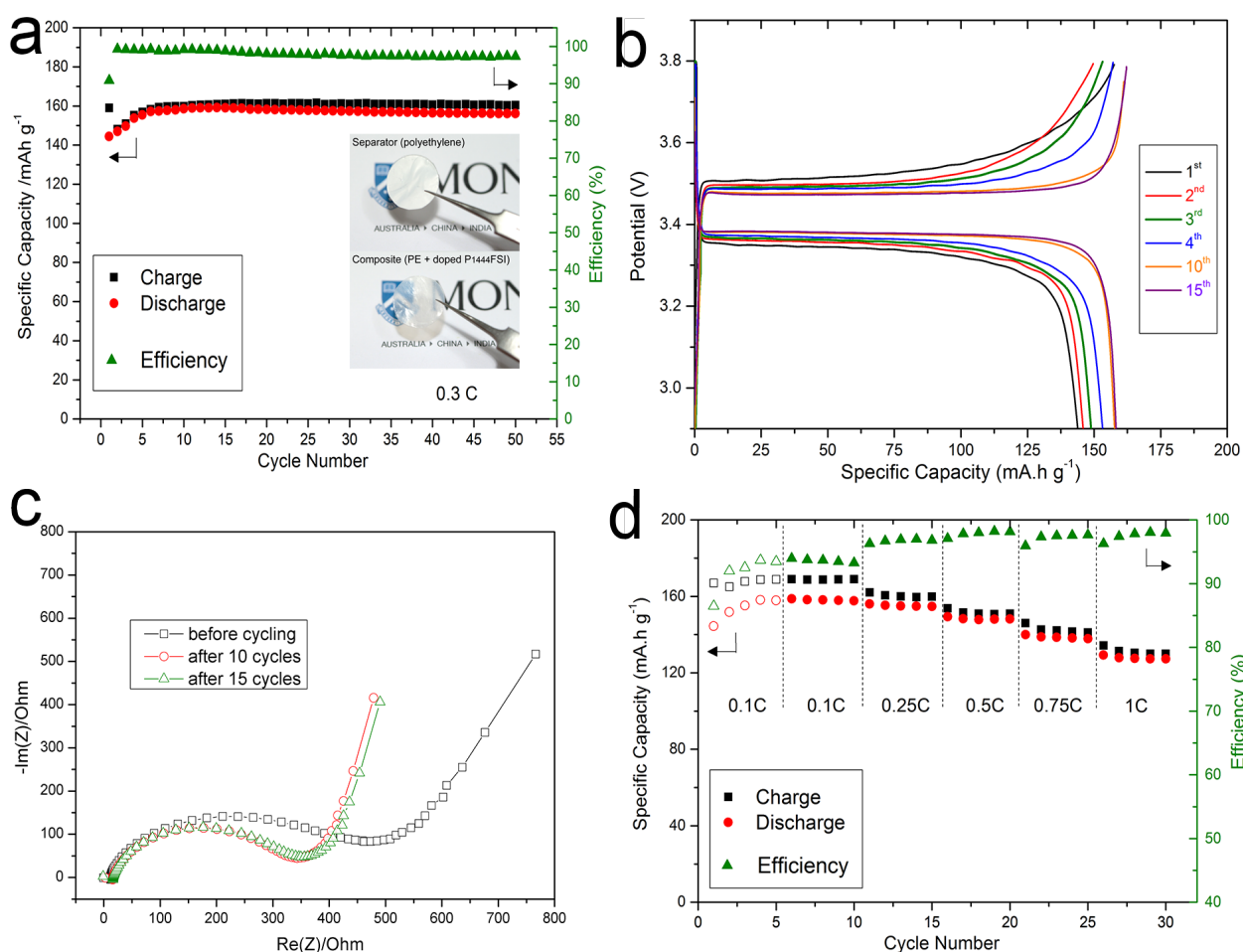


Fig 5. (a) Li|LiFePO₄ cell cycling at 0.3C rate at 30°C using a composite electrolyte (4 mol% LiFSI doped P₁₄₄₄FSI and polyethylene separator, as shown in the inserted image). (b) Charging-discharging profiles for the first four, 10th and 15th cycles of the 50 cycles shown in (a). (c) Nyquist plot of *in-situ* impedance measurements before the first cycle, and after the 10th and 15th cycles. The frequency range was from 1MHz to 0.1Hz. (d) Cell capacity retention (tested with another cell) at charging/discharging rate ranging from 0.1C to 1C. The initial 5 cycles labelled by hollow data points were regarded as preconditioning cycles and there was a 3hour resting time before switching to a higher rate.

The Li⁺/Li redox behaviour of the 4 mol% LiFSI doped P₁₄₄₄FSI is plotted in Figure 4.b. The cyclic voltammetry has been successfully performed using the plastic crystal electrolyte in the solid state at ambient temperature. Moreover, because of the high conductivity at 20 °C, and the good cathodic limit, the lithium plating (reduction) peaks can be fully resolved. Interestingly, in general, in ILs for lithium electrochemistry and specifically for phosphonium based ILs,^{75,76} it has not been possible to fully resolve the lithium reduction peak due to insufficient cathodic stability of the IL resulting from reduction of the IL cation. For the 4 mol% LiFSI doped P₁₄₄₄FSI, when we set the lowest scan cut-off to -0.8 V vs. Li⁺/Li, the reduction or decomposition is observed (shown as a ‘loop’, Fig 4b). Thus, the cut-off was then set to -0.5 V from the second cycle. A repeated experiment with the cut-off set to -0.5 V from the first cycle (Fig S4 of ESI) shows lithium plating and stripping results consistent with those shown in Fig 4.b) Another reduction process also occurs in each cycle at *ca.* 0.4 V vs Li⁺/Li. The intensities of these peaks decreased successively with each cycle, especially from the first to the second cycle. The potential at which this process occurs is consistent

with the onset of reduction in the pure system, as shown in Figure 4.a. It is generally accepted that this behaviour is associated with solid electrolyte interphase (SEI) formation.⁷⁷ Importantly, for good battery performance, the SEI must be stable and support high lithium ion conductivity. In the voltammograms presented in Figure 4.b, there is little further reduction at 0.4 V vs. Li⁺/Li during subsequent cycling. In addition, the reduction currents at the cut-off end (-0.5 V) are decreasing with successive cycles and, most importantly, the estimated lithium redox coulombic efficiency (determined from the ratio of the oxidation and reduction peak areas), jumps from 0.49 to 0.62 after the first cycle and grows to 0.81 by the 9th cycle. This clearly indicates the formation of a stable and effective SEI. In general, the mechanism of formation of the SEI on lithium metal in IL or OIPC based electrolytes is unclear. However, as supported by the observation of a stable and functional SEI in [FSI] based IL | Li systems,^{56-58,78} we believe that the [FSI] anion in this OIPC also exerts an advantageous impact. Furthermore, given the sharp, well defined and fully resolved lithium reduction peaks, which is rarely found in literature, including those based on [FSI] ionic liquids,^{56,78} we

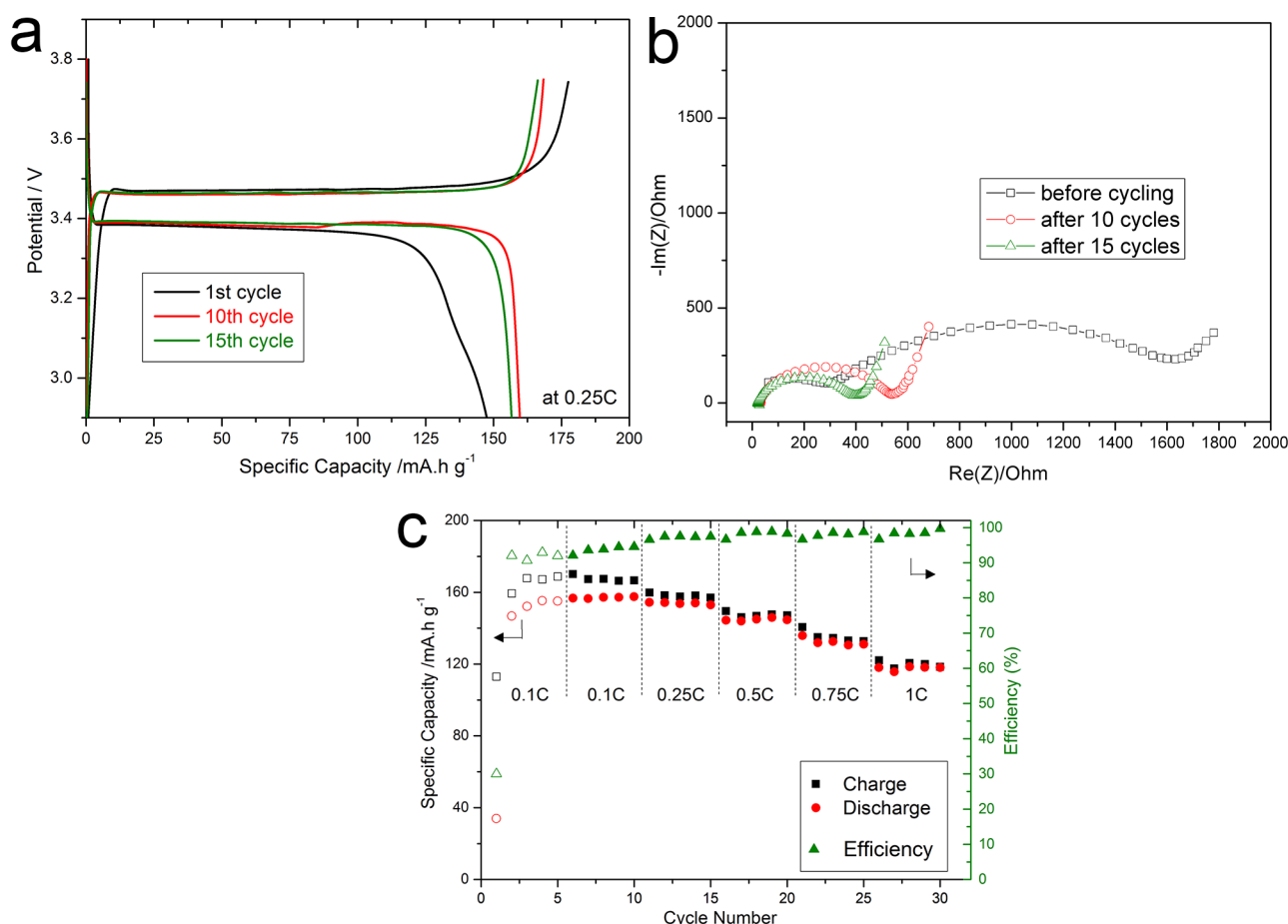


Fig 6. (a) Charging-discharging profiles of Li|LiFePO₄ cell cycling at 0.1C and 20°C using composite electrolyte (4 mol% LiFSI doped P₁₄₄₄FSI and polyethylene separator). (b) The Nyquist plot of *in-situ* impedance measurements before the first cycle, and after the 10th and 15th cycles. The frequency range was from 1MHz to 0.1Hz. (c) The cell capacity retention (tested with another cell) at charging/discharging rate ranging from 0.1C to 1C. The initial 5 cycles labelled by hollow data points were regarded as preconditioning cycles and there was a 3 hour resting time before switching to a higher rate.

also ascribe some of this behaviour to the solid-state properties of the OIPC system: in this system a stable SEI may be derived from the formation of a thin layer of chemically and/or morphologically ‘altered’ solid electrolyte in the closest vicinity to the metal surface, its formation being influenced by solid-state ion diffusion processes and mechanical stresses.^{17,79}

Li | LiFePO₄ plastic crystal cell cycling

Prototypical Li | LiFePO₄ cells have been cycled, using a composite electrolyte consisting of a polyethylene separator and 4 mol% LiFSI doped P₁₄₄₄FSI OIPC (shown in the inset of Figure 5.a). Based on the previous thermal and electrochemical analyses, we performed the cell tests at 30 °C and 20 °C.

The cycling results at 30 °C are presented in Figure 5. Figure 5.a shows the overall cell performance for 50 cycles at a rate of 0.3 C. Although with a relatively low active material loading, the specific charging/discharging capacity climbs to *ca.* 160 mA.h g⁻¹ with *ca.* 99% coulombic efficiency at the 5th cycle, after which the charge capacity is retained for the remaining cycles, with only the discharge capacity declining slightly, to 156 mA.h g⁻¹ and 97% efficiency, by the last cycle. The cycling performance is strongly affected by the SEI formation process

during the first several cycles, during which the discharge capacity steadily increases, accompanied by an efficiency increase from *ca.* 91% to *ca.* 99%. It is also interesting to note a decrease in the internal cell polarisation indicated by the difference between charge and discharge plateaus, shown in Figure 5.b. Corresponding *in-situ* impedance measurements are also plotted in Figure 5.c. This decrease in cell polarisation could originate from several phenomena: first, the SEI formed can act as a conductive “buffer” layer that reduces the solid/solid interfacial resistance, and after the 4th cycle the overpotential is stabilized. Second, with plastic crystal electrolytes we have consistently observed that during initial polarisation cycles (with Li symmetric cells) the internal cell resistance drops substantially, in what we have referred to as the preconditioning process.^{17,19,79} It has been observed that in cycled cells an apparent recrystallization of the OIPC at the interface/interphase region forms smaller grains and hence more grain boundary area, which may contribute to improved conductivity.¹⁷ Finally, because of the Joule heating during the cell cycling process and the effect of lithium dissolution, there may be the formation of more of the melted eutectic phase at the interface, which leads to better electrode wetting and higher

conductivity.

To obtain more information on the utility of the cells with the plastic crystal electrolyte, the capacity and efficiency were recorded at rates from 0.1 C to 1 C (Figure 5.d). The discharge capacity is still greater than *ca.* 150 mAh g⁻¹ at a rate of 0.5 C, and drops to 140 mAh g⁻¹ at 0.75 C and 130 mAh g⁻¹ at 1 C. This remarkable performance is the first example, to our knowledge, of an OIPC electrolyte system performing at practical rates at ambient temperature. The coulombic efficiency surprisingly increases with increasing rate, which may be due to a reduction in irreversible processes at the ‘top of charge’ due to the greater cell polarisation (and hence shorter time in these regions) that occurs with increasing rate.

We then tested fresh cells with exactly the same configuration at a lower temperature of 20 °C, *i.e.* in Phase II. The performance data are gathered in Figure 6. At the rate of 0.1 C, the discharge capacity plateaued at *ca.* 155 mAh g⁻¹ after the 10th cycle (Figure 6.a). This capacity is comparable to that of Li | LiFePO₄ cells containing FSI ionic liquid electrolytes^{61,62} and, to the best of our knowledge, is the highest discharge capacity for Li | LiFePO₄ cells with plastic crystal electrolytes reported so far^{19,20,22,80,81} (including cells running at elevated temperatures). Similar to the cells cycled at 30 °C, we observed the largest irreversible capacity loss on the first cycle. This is consistent with the Li⁺/Li redox behaviour at 20 °C (Figure 4.b). We ascribe the capacity loss to SEI formation, as discussed previously, which could be one of the factors contributing to the high cell capacity achieved. The *in-situ* impedance measurements (Figure 6.b) also suggest an improved interfacial conductivity, showing a dramatic decrease (by more than 1000 Ω) of the interfacial resistance within the initial 10 cycles. It is important to point out that, in contrast to the evolution of interfacial resistance in the cell running at 30 °C and 0.3 C rate (Figure 5.c), the interfacial resistance continues to drop after 10 cycles in the cell running at 20 °C and 0.1 C rate. This very much resembles the preconditioning process discussed previously, associated with recrystallization of the plastic crystal at the Li | plastic crystal interface.¹⁷ Therefore, unlike the cell running at 30 °C where the melted eutectic phase is present, the observation of the preconditioning process in the cell running at 20 °C and at 0.1 C strongly suggests that similar solid-state processes may be occurring in this cell under these conditions. The cell performance at low rates (Figure 6.c) is comparable to that at 30 °C, demonstrating that an effective SEI has been formed. At the higher 1 C rate, however, the discharging capacity (118 mA.h g⁻¹) is lower than that at 30 °C, and appears limited by the bulk conductivity of the electrolyte.

Conclusions

An organic ionic plastic crystal (OIPC) electrolyte P₁₄₄₄FSI has been studied and applied as a solid electrolyte in a safe, high performance prototype lithium battery at ambient temperature. Characterization of the thermal phase behaviour, together with crystal structure information obtained by synchrotron X-ray diffraction, has been compiled to study the OIPC phase/structure environments for the added lithium ions, which plays a key role in understanding the conduction mechanisms that lead to the high conductivity value of 0.26 mS cm⁻¹ at 22 °C. Electrochemical studies of this material indicate a large electrochemical window (*ca.* 6 V).

Importantly, at 20 °C when the material is in the solid state, it is possible to distinctly resolve the Li⁰/Li⁺ redox reaction from which we have direct evidence of formation of a stable and highly conductive solid electrolyte interphase (SEI). We believe that the desired SEI formation is not only caused by the FSI anion chemistry but may also be influenced by the solid nature of the electrolyte. The high ionic conductivity, excellent electrochemical stability and good interfacial properties of the OIPC enabled excellent cycling performance of (Li | LiFePO₄) cells at 30 °C and 20 °C. 160 mAh g⁻¹ discharge capacity was achieved at both 30 °C and 20 °C with 0.1 C rate, which is the highest reported for OIPC based cells to date. At the 1 C rate, the cells retained capacities of approximately 118 mAh g⁻¹ and 130 mAh g⁻¹ at 20 and 30 °C, respectively.

Acknowledgements

The authors gratefully acknowledge funding from the Australian Research Council through its Centre of Excellence program and also for Fellowship support for L. Jin (Sir James McNeil PG Research Scholarship and IPRS) and M. Forsyth and D. R. MacFarlane (Laureate Fellows). We also acknowledge Y. He for the supply of cathode materials and A. F. Hollenkamp for valuable discussions. This research was undertaken on the powder diffraction beamline with assistance from beamline scientist H. Brand at the Australian Synchrotron, Victoria, Australia.

Notes and references

1. D. Cardwell, *New York Times*, 2013, B2.
2. M. Armand, F. Endres, D. R. MacFarlane, H. Ohno, and B. Scrosati, *Nat Mater*, 2009, **8**, 621–629.
3. B. Scrosati, J. Hassoun, and Y.-K. Sun, *Energy Environ. Sci.*, 2011, **4**, 3287.
4. D. R. MacFarlane, N. Tachikawa, M. Forsyth, J. M. Pringle, P. C. Howlett, G. D. Elliott, J. H. Davis, M. Watanabe, P. Simon, and C. A. Angell, *Energy Environ. Sci.*, 2013.
5. D. R. MacFarlane, J. Huang, and M. Forsyth, *Nature*, 1999, **402**, 792–794.
6. D. R. MacFarlane and M. Forsyth, *Adv. Mater.*, 2001, **13**, 957–966.
7. J. M. Pringle, P. C. Howlett, D. R. MacFarlane, and M. Forsyth, *J. Mater. Chem.*, 2010, **20**, 2056.
8. J. M. Pringle, *Phys. Chem. Chem. Phys.*, 2013, **15**, 1339.
9. T. Shimizu, S. Tanaka, N. Onoda-Yamamuro, S. Ishimaru, and R. Ikeda, *Faraday Trans.*, 1997, **93**, 321–326.
10. J. Timmermans, *Journal of Physics and Chemistry of Solids*, 1961, **18**, 1–8.
11. D. R. MacFarlane, P. Meakin, J. Sun, N. Amini, and M. Forsyth, *J. Phys. Chem. B*, 1999, **103**, 4164–4170.
12. Z.-B. Zhou and H. Matsumoto, *Electrochem. Commun.*, 2007, **9**, 1017–1022.
13. M. Völz, P.-J. Alarco, Y. Abu-Lebdeh, and M. Armand, *ChemPhysChem*, 2004, **5**, 1027–1033.
14. A. Abouimrane, Y. Abu-Lebdeh, P.-J. Alarco, and M. Armand, *J. Electrochem. Soc.*, 2004, **151**, A1028.
15. P. C. Howlett, J. Sunarso, Y. Shekibi, E. Wasser, L. Jin, D. R. MacFarlane, and M. Forsyth, *Solid State Ionics*, 2011, **204–205**, 73–79.
16. P. J. Alarco, Y. Abu-Lebdeh, N. Ravet, and M. Armand, *Solid State Ionics*, 2004, **172**, 53–56.
17. L. Jin, P. Howlett, J. Efthimiadis, M. Kar, D. Macfarlane, and M. Forsyth, *J. Mater. Chem.*, 2011, **21**, 10171–10178.
18. W. A. Henderson, D. M. Seo, Q. Zhou, P. D. Boyle, J.-H. Shin, H. C. De Long, P. C. Trulove, and S. Passerini, *Adv. Energy Mater.*, 2012, **2**, 1343–1350.

19. J. Sunarso, Y. Shekibi, J. Efthimiadis, L. Jin, J. Pringle, A. Hollenkamp, D. MacFarlane, M. Forsyth, and P. Howlett, *J Solid State Electrochem*, 2012, **16**, 1841–1848.
20. Y. Shekibi, T. R  ther, J. Huang, and A. F. Hollenkamp, *Phys. Chem. Chem. Phys.*, 2012, **14**, 4597.
21. Y. Abu-Lebdeh, A. Abouimrane, P.-J. Alarco, and M. Armand, *J. Power Sources*, 2006, **154**, 255–261.
22. H. Yoon, G. H. Lane, Y. Shekibi, P. C. Howlett, M. Forsyth, A. S. Best, and D. R. MacFarlane, *Energy Environ. Sci.*, 2013, **6**, 979.
23. L.-Z. Fan, X.-L. Wang, and F. Long, *J. Power Sources*, 2009, **189**, 775–778.
24. J. Chen, T. Peng, K. Fan, R. Li, and J. Xia, *Electrochimica Acta*, 2013, **94**, 1–6.
25. R. Taniki, K. Matsumoto, T. Nohira, and R. Hagiwara, *J. Power Sources*, 2014, **245**, 758–763.
26. Y. Abu-Lebdeh, A. Abouimrane, P. J. Alarco, A. Hammami, L. Ionescu-Vasii, and M. Armand, *Electrochem. Commun.*, 2004, **6**, 432–434.
27. U. A. Rana, R. Vijayaraghavan, D. R. MacFarlane, and M. Forsyth, *Chem. Commun.*, 2011, **47**, 6401.
28. S. Long, P. Howlett, D. MacFarlane, and M. Forsyth, *Solid State Ionics*, 2006, **177**, 647–652.
29. J. Luo, O. Conrad, and I. F. J. Vankelecom, *J. Mater. Chem. A*, 2013, **1**, 2238.
30. H. Zhu, U. A. Rana, V. Ranganathan, L. Jin, L. A. O'Dell, D. R. MacFarlane, and M. Forsyth, *J. Mater. Chem. A*, 2013, **2**, 681.
31. U. A. Rana, P. M. Bayley, R. Vijayaraghavan, P. Howlett, D. R. MacFarlane, and M. Forsyth, *Phys. Chem. Chem. Phys.*, 2010, **12**, 11291.
32. Q. Li, J. Zhao, B. Sun, B. Lin, L. Qiu, Y. Zhang, X. Chen, J. Lu, and F. Yan, *Adv. Mater.*, 2012, **24**, 945–950.
33. P. Wang, Q. Dai, S. M. Zakeeruddin, M. Forsyth, D. R. MacFarlane, and M. Gr  tzel, *J. Am. Chem. Soc.*, 2004, **126**, 13590–13591.
34. D. Hwang, D. Y. Kim, S. M. Jo, V. Armel, D. R. MacFarlane, D. Kim, and S.-Y. Jang, *Sci. Rep.*, 2013, **3**.
35. S. Li, L. Qiu, C. Shi, X. Chen, and F. Yan, *Adv. Mater.*, 2014, **26**, 1266–1271.
36. Q. Li, X. Chen, J. Zhao, L. Qiu, Y. Zhang, B. Sun, and F. Yan, *J. Mater. Chem.*, 2012, **22**, 6674.
37. V. Armel, M. Forsyth, D. R. MacFarlane, and J. M. Pringle, *Energy Environ. Sci.*, 2011, **4**, 2234.
38. E. I. Cooper and C. A. Angell, *Solid State Ionics*, 1986, **18–19**, Part 1, 570–576.
39. M. Lee, U. H. Choi, S. Wi, C. Slebodnick, R. H. Colby, and H. W. Gibson, *J. Mater. Chem.*, 2011, **21**, 12280.
40. V. Armel, D. Velayutham, J. Sun, P. C. Howlett, M. Forsyth, D. R. MacFarlane, and J. M. Pringle, *J. Mater. Chem.*, 2011, **21**, 7640.
41. J. Janikowski, M. R. Razali, C. M. Forsyth, K. M. Nairn, S. R. Batten, D. R. MacFarlane, and J. M. Pringle, *ChemPlusChem*, 2013, **78**, 486–497.
42. J. E. Puskas, Y. Kwon, P. Antony, and A. K. Bhowmick, *J. Polym. Sci. A Polym. Chem.*, 2005, **43**, 1811–1826.
43. R. Taniki, K. Matsumoto, R. Hagiwara, K. Hachiya, T. Morinaga, and T. Sato, *J. Phys. Chem. B*, 2013, **117**, 955–960.
44. J. M. Pringle, J. Adebahr, D. R. MacFarlane, and M. Forsyth, *Phys. Chem. Chem. Phys.*, 2010, **12**, 7234.
45. W. M. Reichert, J. D. Holbrey, R. P. Swatloski, K. E. Gutowski, A. E. Visser, M. Nieuwenhuyzen, K. R. Seddon, and R. D. Rogers, *Crystal Growth & Design*, 2007, **7**, 1106–1114.
46. A. J. Seeber, M. Forsyth, C. M. Forsyth, S. A. Forsyth, G. Annat, and D. R. MacFarlane, *Phys. Chem. Chem. Phys.*, 2003, **5**, 2692.
47. G. Annat, J. Adebahr, I. R. McKinnon, D. R. MacFarlane, and M. Forsyth, *Solid State Ionics*, 2007, **178**, 1065–1071.
48. Z.-B. Zhou, H. Matsumoto, and K. Tatsumi, *Chem. Eur. J.*, 2006, **12**, 2196–2212.
49. J. Janikowski, C. Forsyth, D. R. MacFarlane, and J. M. Pringle, *J. Mater. Chem.*, 2011, **21**, 19219.
50. K. Tsunashima and M. Sugiya, *Electrochem. Commun.*, 2007, **9**, 2353–2358.
51. K. J. Fraser and D. R. MacFarlane, *Aust. J. Chem.*, 2009, **62**, 309.
52. C. J. Bradaric, A. Downard, C. Kennedy, A. J. Robertson, and Y. Zhou, *Green Chem.*, 2002, **5**, 143–152.
53. C. Michot, M. Armand, J. Y. Sanchez, Y. Choquette, and M. Gauthier, 1994.
54. C. Michot, M. Armand, M. Gauthier, and N. Ravet, 1999.
55. J. K. Ruff, *Inorg Chem*, 1965, **4**, 1446–1449.
56. A. I. Bhatt, A. S. Best, J. Huang, and A. F. Hollenkamp, *J. Electrochem. Soc.*, 2010, **157**, A66.
57. E. Paillard, Q. Zhou, W. A. Henderson, G. B. Appetecchi, M. Montanino, and S. Passerini, *J. Electrochem. Soc.*, 2009, **156**, A891.
58. A. Budi, A. Basile, G. Opletal, A. F. Hollenkamp, A. S. Best, R. J. Rees, A. I. Bhatt, A. P. O'Mullane, and S. P. Russo, *J. Phys. Chem. C*, 2012, **116**, 19789–19797.
59. H. Matsumoto, H. Sakaebe, K. Tatsumi, M. Kikuta, E. Ishiko, and M. Kono, *J. Power Sources*, 2006, **160**, 1308–1313.
60. A. Guerfi, S. Duchesne, Y. Kobayashi, A. Vijh, and K. Zaghib, *J. Power Sources*, 2008, **175**, 866–873.
61. A. P. Lewandowski, A. F. Hollenkamp, S. W. Donne, and A. S. Best, *J. Power Sources*, 2010, **195**, 2029–2035.
62. A. Guerfi, M. Dontigny, Y. Kobayashi, A. Vijh, and K. Zaghib, *J Solid State Electrochem*, 2008, **13**, 1003–1014.
63. P. Atkins, *Inorganic Chemistry*, W. H. Freeman and Company, New York, 5 edn. 2010.
64. N. G. Tsierkezos, *J Solution Chem*, 2007, **36**, 289–302.
65. M. Forsyth, T. Chimdi, A. Seeber, D. Gunzelmann, and P. C. Howlett, *J. Mater. Chem. A*, 2014, **2**, 3993.
66. W. A. Henderson and S. Passerini, *Chem. Mater.*, 2004, **16**, 2881–2885.
67. M. Forsyth, J. Huang, and D. R. MacFarlane, *J. Mater. Chem.*, 2000, **10**, 2259–2265.
68. A. I. Bhatt, I. May, V. A. Volkovich, M. E. Hetherington, B. Lewin, R. C. Thied, and N. Ertok, *J. Chem. Soc., Dalton Trans.*, 2002, 4532–4534.
69. K. Tsunashima and M. Sugiya, *Electrochemistry (Tokyo)*, 2007, **75**, 734.
70. P. Bonhote, A.-P. Dias, N. Papageorgiou, K. Kalyanasundaram, and M. Gr  tzel, *Inorg Chem*, 1996, **35**, 1168–1178.
71. H. Sakaebe and H. Matsumoto, *Electrochem. Commun.*, 2003, **5**, 594–598.
72. H.-B. Han, K. Liu, S.-W. Feng, S.-S. Zhou, W.-F. Feng, J. Nie, H. Li, X.-J. Huang, H. Matsumoto, and M. Armand, *Electrochimica Acta*, 2010, **55**, 7134–7144.
73. J. B. Goodenough and K.-S. Park, *J. Am. Chem. Soc.*, 2013, **135**, 1167–1176.
74. J. B. Goodenough and Y. Kim, *Chem. Mater.*, 2010, **22**, 587–603.
75. K. Tsunashima and M. Sugiya, *Electrochem. Solid-State Lett.*, 2008, **11**, A17.
76. K. Tsunashima, Y. Sakai, and M. Matsumiya, *Electrochem. Commun.*, 2014, **39**, 30–33.
77. E. Peled, *J. Electrochem. Soc.*, 1979, **126**, 2047–2051.
78. A. S. Best, A. I. Bhatt, and A. F. Hollenkamp, *J. Electrochem. Soc.*, 2010, **157**, A903.
79. P. C. Howlett, Y. Shekibi, D. R. MacFarlane, and M. Forsyth, *Adv. Eng. Mater.*, 2009, **11**, 1044–1048.
80. A. Abouimrane, P.-J. Alarco, Y. Abu-Lebdeh, I. Davidson, and M. Armand, *J. Power Sources*, 2007, **174**, 1193–1196.
81. A. Abouimrane and I. J. Davidson, *J. Electrochem. Soc.*, 2007, **154**, A1031.